

Design Optimization of Three-Dimensional Wire Arrangement Considering Wire Crossings for Tendon-driven Robots

Kento Kawaharazuka¹, Shintaro Inoue¹, Yuta Sahara¹, Keita Yoneda¹, Temma Suzuki¹, and Kei Okada¹

Abstract—Tendon-driven mechanisms are useful from the perspectives of variable stiffness, redundant actuation, and lightweight design, and they are widely used, particularly in hands, wrists, and waists of robots. The design of these wire arrangements has traditionally been done empirically, but it becomes extremely challenging when dealing with complex structures. Various studies have attempted to optimize wire arrangement, but many of them have oversimplified the problem by imposing conditions such as restricting movements to a 2D plane, keeping the moment arm constant, or neglecting wire crossings. Therefore, this study proposes a three-dimensional wire arrangement optimization that takes wire crossings into account. We explore wire arrangements through a multi-objective black-box optimization method that ensures wires do not cross while providing sufficient joint torque along a defined target trajectory. For a 3D link structure, we optimize the wire arrangement under various conditions, demonstrate its effectiveness, and discuss the obtained design solutions.

I. INTRODUCTION

Various tendon-driven robots have been developed to date. These range from biomimetic robots that closely mimic the human skeleton and muscles [1]–[3] to non-biomimetic robots that effectively leverage the advantages of wires [4]–[7]. Tendon-driven mechanisms offer several useful characteristics, such as redundant actuation enabling continued operation even when one wire breaks, variable stiffness control through hardware, and lightweight design of the distal end by allowing all actuators to be arranged in the root link. These features are being effectively utilized, especially in areas such as hands, wrists, and waists. However, the design, particularly the wire arrangement, is still mostly done empirically, and designing becomes extremely difficult as the structure becomes more complex.

In response to this, various attempts have been made to optimize wire arrangement. These wire arrangement optimization methods can be broadly categorized into two conditions: constant moment arm and variable moment arm. The constant moment arm refers to systems in which pulleys are placed at the joints, and the distance from the wire to the joint center remains constant. In the constant moment arm condition, the optimization mainly focuses on the radius and spacing of the pulleys, which correspond to the muscle Jacobian. In [8], the muscle Jacobian is numerically optimized to secure a torque space equivalent to that of a human hand for robotic fingers. In [9], the presence or absence of moment arms for each muscle is optimized for a musculoskeletal

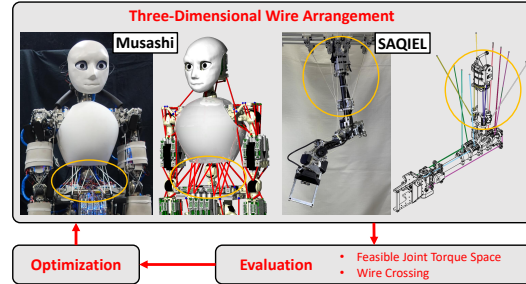


Fig. 1. The concept of this study: complex three-dimensional wire arrangement can be optimized with multi-objective optimization considering the wire crossings and feasible joint torque space. The figures show the waist of tendon-driven musculoskeletal humanoid Musashi [3] and the shoulder of light-weight safe manipulator SAQIEL [6] that we have developed so far.

robot with an exhaustive search. In [10], the pulley radius, elasticity, and pre-tension are optimized for the design of asymmetric compliance actuators. In [11], the spacing between the two fingers, pulley radius, and pulley spacing are optimized for a two-fingered hand by a genetic algorithm. In [12] the muscle Jacobian is optimized for a musculoskeletal robot using a genetic algorithm, ensuring continued operation even if one muscle is severed. In [13], the pulley radius, link length, and pre-tension of the tendon-driven underactuated robot are optimized using reinforcement learning.

In the variable moment arm condition, the positions of the start point, relay points, and end points of the wires are optimized. In [14], the distance between joints and wires is optimized to enlarge the feasible joint angle space for continuum robots. In [15], the wire attachment points of a Cable-Driven Parallel Robot (CDPR) is optimized for upper limb rehabilitation based on evolutionary computation and multiple objective functions. In [16], the tension and wire attachment points are numerically optimized for the stiffness adjustment of CDPR. In [17], the positions of start points and end points of wires are optimized for a musculoskeletal robot to construct a constraint force field. In [18], a complex wire arrangement optimization method that includes not only start and end points but also relay points of wires is proposed.

On the other hand, many of the previously introduced studies focus on cases where the moment arm is constant [8]–[13] or a planar motion is assumed [14], [17], [18]. While wire arrangement optimization in three-dimensional spaces with variable moment arms has been conducted for CDPR [14]–[16], these studies do not consider wire crossings. They fine-tune the wire positions under the assumption that wire crossings do not occur in a large space. In other words, many methods have simplified the problem of wire arrangement optimization. However, in reality, there are numerous com-

¹ The authors are with the Department of Mechano-Informatics, Graduate School of Information Science and Technology, The University of Tokyo, 7-3-1 Hongo, Bunkyo-ku, Tokyo, 113-8656, Japan. [kawaharazuka, s-inoue, sahara, yoneda, t-suzuki, k-okada]@jsk.imi.i.u-tokyo.ac.jp

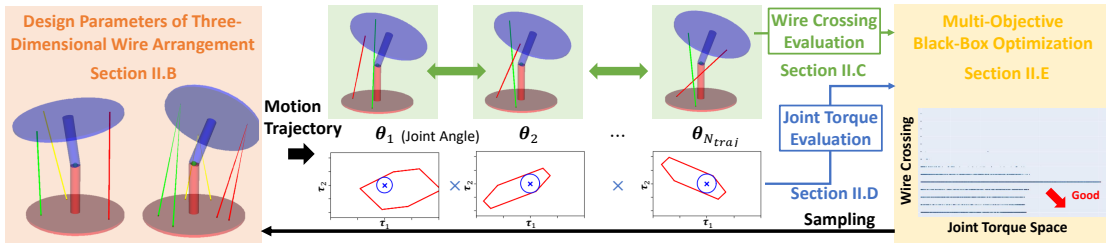


Fig. 2. The overview of the three-dimensional wire arrangement optimization considering wire crossings and feasible joint torque space.

plex structures where the system is three-dimensional, the moment arms are variable, and wire crossings do occur [1]–[3], [6]. For example, the shoulder of SAQIEL [6] and the waist of Musashi [3] shown in Fig. 1 face significant issues with wire crossings during rotation in the yaw direction. Similarly, this issue occurs in the freely configurable wire arrangement of the mobile tendon-driven robot CubiX [7], as well as in the shoulder, waist, and hip joints of most other musculoskeletal humanoids [1], [2]. When wires cross, not only can they become tangled and destabilize the structure, but the friction may also increase the risk of wire breakage. It is necessary to explore wire arrangements that prevent multiple wires from crossing within a small space, while still allowing for controllable and sufficient joint torque.

In this study, we propose a three-dimensional wire arrangement optimization method that takes wire crossings into account (Fig. 1). We define a target trajectory and perform multi-objective black-box optimization to explore wire arrangements that prevent wire crossings along the trajectory while ensuring a stable joint torque space. We optimize wire arrangements under various conditions for a three-dimensional link structure, demonstrating the effectiveness of the method and discussing the resulting design solutions.

II. DESIGN OPTIMIZATION OF THREE-DIMENSIONAL WIRE ARRANGEMENT CONSIDERING WIRE CROSSINGS

A. Overview of Wire Arrangement Optimization

As in Fig. 2, we describe the design parameters of the wire arrangement in Section II-B, the method for detecting wire crossings in Section II-C, the calculation method of feasible joint torque in Section II-D, and the multi-objective optimization method in Section II-E. We briefly outline the problem setting addressed in this study. The body structure considered is a two-link three-dimensional structure, as shown on the left side of Fig. 2. By placing the start, relay, and end points of the wires on each link, this structure is actuated. The task is to achieve a given joint angle trajectory. Therefore, a sequence of joint angles $\{\theta_1, \theta_2, \dots, \theta_{N_{traj}}\}$ is provided. N_{traj} represents the number of joint angle sequences, and θ_i is a D -dimensional vector, where D is the number of DOFs of the joint. Here, it is required that no wire crossings occur along the trajectory and that sufficient feasible joint torque is ensured. The goal of this study is to explore a wire arrangement that satisfies these conditions.

B. Design Parameters of Wire Arrangement

The detailed link structure addressed in this study and an example of wire arrangement are shown in Fig. 3. This

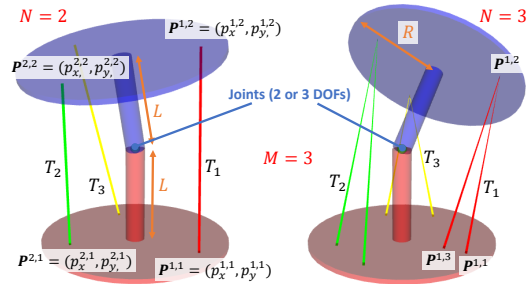


Fig. 3. The design parameters of wire arrangement.

structure consists of two primary links with joints that have 2-3 degrees of freedom (DOFs), and it can be seen as a direct extension of the general two-dimensional link structures of tendon-driven robots into three dimensions. Each link is divided into a long cylindrical section with length L and a larger circular section with radius R , where the start, relay, and end points of the wires can be placed. We arrange M wires on the structure, with each wire having N start, relay, and end points. Fig. 3 shows an example of wire arrangement with $M = 3$ and $N = \{2, 3\}$. The position of the j -th relay point on the i -th wire is represented as $P^{i,j} = (p_x^{i,j}, p_y^{i,j})$. When $N = 2$, each wire connects the links in a straight line, while for $N = 3$, a foldback occurs, and the start and end points are placed on the same link. Thus, the design parameters for the wire arrangement in this study consist of $2 \times N \times M$ continuous values $\{p_x^{i,j}, p_y^{i,j}\}$, where $1 \leq i \leq M$ and $1 \leq j \leq N$. The range of $p_{\{x,y\}}^{i,j}$ is constrained to the surface of the larger circular section as follows.

$$-R \leq p_x^{i,j} \leq R \quad (1)$$

$$-\sqrt{R^2 - (p_x^{i,j})^2} \leq p_y^{i,j} \leq \sqrt{R^2 - (p_x^{i,j})^2} \quad (2)$$

C. Detection of Wire Crossings

First, we consider the minimum distance between two wires. Let the start point of one wire at joint angle θ_i be \mathbf{a}_1 and the end point be \mathbf{a}_2 , and the start point of the other wire be \mathbf{b}_1 and the end point be \mathbf{b}_2 . For simplicity, we do not use the notation $P^{i,j}$ here. Each wire segment and the distance between the two wires can be represented using parameters s and t ($0 \leq s, t \leq 1$) as follows.

$$\mathbf{p}_a(s) = \mathbf{a}_1 + s \cdot (\mathbf{a}_2 - \mathbf{a}_1) \quad (3)$$

$$\mathbf{p}_b(t) = \mathbf{b}_1 + t \cdot (\mathbf{b}_2 - \mathbf{b}_1) \quad (4)$$

$$\begin{aligned} d(s, t) &= \|\mathbf{p}_a(s) - \mathbf{p}_b(t)\|_2 \\ &= \|\mathbf{a}_1 + s \cdot \mathbf{u} - (\mathbf{b}_1 + t \cdot \mathbf{v})\|_2 \\ &= \|\mathbf{w} + s \cdot \mathbf{u} - t \cdot \mathbf{v}\|_2 \end{aligned} \quad (5)$$

where $\mathbf{u} = \mathbf{a}_2 - \mathbf{a}_1$, $\mathbf{v} = \mathbf{b}_2 - \mathbf{b}_1$, and $\mathbf{w} = \mathbf{a}_1 - \mathbf{b}_1$, and $\|\cdot\|_2$ denotes the L2 norm. To find the values of s and t that minimize $d(s, t)$, we differentiate $d(s, t)$ with respect to s and t , and solve for the points where these partial derivatives are zero.

$$\frac{\partial d(s, t)}{\partial s} = 2\mathbf{u} \cdot (\mathbf{w} + s \cdot \mathbf{u} - t \cdot \mathbf{v}) = 0 \quad (6)$$

$$\frac{\partial d(s, t)}{\partial t} = -2\mathbf{v} \cdot (\mathbf{w} + s \cdot \mathbf{u} - t \cdot \mathbf{v}) = 0 \quad (7)$$

By solving this system of equations, we can compute the values of s_c and t_c that minimize $d(s, t)$ as follows,

$$s_c = \frac{be - cd}{ac - b^2}, t_c = \frac{ae - bd}{ac - b^2} \quad (8)$$

where $a = \mathbf{u} \cdot \mathbf{u}$, $b = \mathbf{u} \cdot \mathbf{v}$, $c = \mathbf{v} \cdot \mathbf{v}$, $d = \mathbf{u} \cdot \mathbf{w}$, and $e = \mathbf{v} \cdot \mathbf{w}$. Finally, considering the constraints on s and t , the minimum distance s_c^* and t_c^* are calculated as follows.

$$s_c^* = \max(0, \min(1, s_c)) \quad (9)$$

$$t_c^* = \max(0, \min(1, t_c)) \quad (10)$$

The minimum distance between the two wires is then given by $d^* = d(s_c^*, t_c^*)$.

Next, we consider the trajectory from θ_i to θ_{i+1} , and determine whether the wires cross during this movement. To determine if two wires cross or touch, we check whether there is any point along the trajectory where $d^* < \epsilon$ (where ϵ is a sufficiently small constant, set to 1.0×10^{-4} in this study). The start and end points of the two wires at a certain point on the trajectory are computed as follows,

$$\begin{aligned} \mathbf{a}_1^k &= k\mathbf{a}_1 + (1-k)\mathbf{a}_1' & \mathbf{a}_2^k &= k\mathbf{a}_2 + (1-k)\mathbf{a}_2' \\ \mathbf{b}_1^k &= k\mathbf{b}_1 + (1-k)\mathbf{b}_1' & \mathbf{b}_2^k &= k\mathbf{b}_2 + (1-k)\mathbf{b}_2' \end{aligned}$$

where k is a continuous parameter ($0 \leq k \leq 1$), and $\{\mathbf{a}, \mathbf{b}\}'_{\{1,2\}}$ represent the start and end points of the wires at θ_{i+1} . Ideally, we should compute $\{\mathbf{a}, \mathbf{b}\}^k_{\{1,2\}}$ for each point along the trajectory from θ_i to θ_{i+1} , but for computational efficiency, we approximate them using linear interpolation between $\{\mathbf{a}, \mathbf{b}\}_{\{1,2\}}$ and $\{\mathbf{a}, \mathbf{b}\}'_{\{1,2\}}$. By dividing the parameter k and checking if $d^* < \epsilon$ at each step, we can detect wire crossings. However, setting ϵ appropriately is challenging; improper settings may fail to detect wire crossings. Similarly, setting the number of divisions for k is also difficult; if the divisions are too coarse, there may be a failure to detect wire crossings, while if they are too fine, the computational cost becomes enormous. To avoid manually setting ϵ and the number of divisions for k , we utilize the fact that d^* is convex downwards and employ Brent's method [19], a root-finding algorithm, to search for k where $d^* < \epsilon$. If the maximum number of iterations (set to 20 in this study) is exceeded without converging to a solution where $d^* < \epsilon$, we conclude that no wire crossing occurs.

So far, we have discussed wire crossings between two wires. In practice, this is done for all possible combinations of wires. If there is a foldback, we also check whether different segments of the same wire cross. Additionally, to ensure that the wires do not cross the joints, we perform

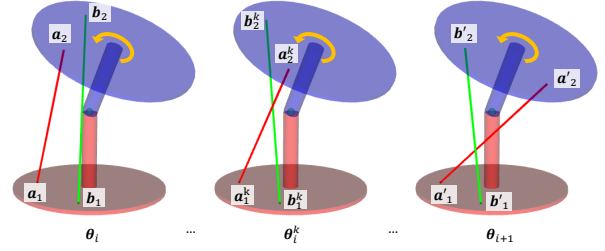


Fig. 4. The configuration detecting wire crossings.

similar calculations to detect intersections between the wire segments and the joint link segments.

D. Joint Torque Evaluation

We describe the method for calculating feasible joint torque along the given trajectory. To reduce computational complexity, the feasible joint torque is calculated only at the waypoints θ_i ($1 \leq i \leq N_{traj}$) rather than along the entire trajectory. In tendon-driven systems, the following equation generally holds,

$$\boldsymbol{\tau} = -\mathbf{G}^T(\boldsymbol{\theta})\mathbf{f} \quad (11)$$

where \mathbf{f} , $\boldsymbol{\tau}$, and $\mathbf{G}(\boldsymbol{\theta})$ represent the muscle tension, joint torque, and muscle Jacobian, respectively. The vector \mathbf{f} is an M -dimensional vector, and $\boldsymbol{\tau}$ is a D -dimensional vector. The space of muscle tensions can be expressed as follows.

$$F := \{\mathbf{f} \in \mathbb{R}^M \mid \mathbf{f}^{min} \leq \mathbf{f} \leq \mathbf{f}^{max}\} \quad (12)$$

By transforming F using Eq. 11, the joint torque space T can be obtained as follows.

$$T := \{\boldsymbol{\tau} \in \mathbb{R}^N \mid \exists \mathbf{f} \in F, \boldsymbol{\tau} = -\mathbf{G}^T \mathbf{f}\} \quad (13)$$

To maintain a given joint angle θ_i , it is necessary to generate joint torques in all directions at that state. This requires that a hypersphere B with a radius R_B ($R_B > 0$) and centered at the origin is inscribed within the joint torque space T . Conversely, if the origin lies outside of T , it indicates that sufficient joint torque cannot be generated.

We now describe how to determine whether the origin lies within T , and if so, how to calculate the radius R_B of the inscribed hypersphere. First, we extract all the vertices of the hypercube F formed by \mathbf{f} and project them into the joint torque space T . We then compute the convex hull C of all the projected vertices. To check whether the origin is inside C , we compute the signed distance d_C from the origin to all the hyperplanes of C . If the origin is inside C , all d_C values are negative. Therefore, if the maximum value of d_C is zero or greater, the origin is not inside C . If the origin is inside C , the minimum absolute value of d_C represents the radius R_B of the inscribed hypersphere. Although the effect of gravity is not directly considered in this study, if gravity were to be considered, the origin of the hypersphere can be shifted to the gravity compensation torque value.

E. Multi-Objective Black-Box Optimization

The wire arrangement is optimized using multi-objective black-box optimization. For the current wire arrangement, the evaluation functions are set based on the number of wire crossings along the trajectory and the feasible joint torque. The optimization aims to minimize the former and maximize the latter. The evaluation functions are defined as follows,

$$E_{cross} = \sum h_{cross}(d^* < \epsilon) \quad (14)$$

$$E_{torque} = \prod h_{torque}(C) \quad (15)$$

where h_{cross} is a function that returns 1 if a wire crossing occurs and 0 otherwise, and E_{cross} represents the total number of wire crossings along the trajectory. Also, h_{torque} returns R_{min} (1.0×10^{-3} in this study) if the origin is not inside C , and R_B if the origin is inside C . E_{torque} represents the product of the radii of the inscribed hyperspheres of feasible joint torque at all waypoints along the trajectory. Using the product ensures that R_B is uniformly maximized across all postures. While it is also possible to use the summation, this approach may result in optimization where R_B is maximized for certain postures but minimized for others. Using these two evaluation functions, we optimize the wire arrangement with NSGA-II, a multi-objective optimization algorithm implemented in the black-box optimization library Optuna [20]. NSGA-II is chosen for its ability to handle multi-objective optimization and its relatively large recommended sample size. For all experiments, the number of iterations is set to 30,000. The optimization took approximately two hours for $N = 2$, $M = 3$, and $D = 2$, and seven hours for $N = 3$, $M = 6$, and $D = 3$.

III. SIMULATION EXPERIMENTS

A. Experimental Setup

We describe the experimental setup of this study. The 3D link structure was set with parameters $R = 0.2$ [m] and $L = 0.2$ [m], and the muscle tension limits were set as $f^{min} = 1.0$ [N] and $f^{max} = 200$ [N]. The number of joints was either 2-DOF or 3-DOF, where the 2-DOF joints included roll and yaw joints, and the 3-DOF joints included roll, pitch, and yaw joints. The number of wires was set to $M = \{3, 4\}$ for the 2-DOF joints and $M = \{4, 5, 6\}$ for the 3-DOF joints, and the number of relay points was set to $N = \{2, 3\}$.

The joint angle trajectories were set as follows: for the 2-DOF joints, $\{(30, 30), (-30, 30), (-30, -30), (30, -30)\}$ [deg]; and for the 3-DOF joints, $\{(20, 20, 30), (20, 20, -30), (-20, 20, -30), (-20, 20, 30), (-20, -20, 30), (-20, -20, -30), (20, -20, -30), (20, -20, 30)\}$ [deg]. In this study, the trajectory covers a wide range of motion evenly, but task-specific trajectories could also be used.

Here, we explain how to interpret the results using Fig. 5. This figure shows the experimental results for the 2-DOF joints with 3 wires and 2 or 3 relay points. The topmost graph displays the sampling results from the optimization process, with the x -axis representing E_{torque} and the y -axis representing E_{cross} . Lighter colored points show initial solutions, while darker colored points show final solutions.

The solutions located in the lower right part of the graph are the better solutions. Among the Pareto solutions, the design with $E_{cross} = 0$ (i.e., no wire crossings) is labeled as Design-1, and the design with $E_{cross} > 0$ and the largest E_{torque} is labeled as Design-2. Similarly, when $N = 3$, the designs are labeled as Design-1' and Design-2', respectively. For these designs, the lower part of the figure shows the motion of the robots and the graphs of the feasible joint torque regions. ①–④ show the robots at the joint angles $\{\theta_1, \dots, \theta_4\}$ from side and top views. $E_{cross}^{i \rightarrow i+1}$ indicates the number of wire crossings along the trajectory from θ_i to θ_{i+1} . Note that what may appear as a crossing between wires or between a wire and a link from one view often does not represent an actual crossing when viewed from another perspective. The feasible joint torque region for each joint angle is shown in the graph, with the x -axis representing the torque in the roll direction and the y -axis representing the torque in the yaw direction. The convex hull C in Section II-D is shown by the red line, and the inscribed hypersphere B is shown by the blue line. E_{torque}^i indicates the radius R_B of the inscribed hypersphere of the feasible joint torque at θ_i . For the 3-DOF joints, ①–⑧ show the robots at the joint angles $\{\theta_1, \dots, \theta_8\}$, and the feasible joint torque region is plotted with the x -axis as the roll direction and the y -axis as the yaw direction, with the pitch torque not shown. In other words, the 3D convex hull C and the inscribed hypersphere B are projected onto a 2D plane.

B. 2-DOF Joint Experiments

Fig. 5 shows the results for $N = \{2, 3\}$ and $M = 3$, while Fig. 6 shows the results for $N = \{2, 3\}$ and $M = 4$. From the sampling results, we can observe several Pareto solutions for both cases. Each of these includes solutions with no wire crossings, indicated by $E_{cross} = 0$. Additionally, we can see that allowing wire crossings leads to design solutions with larger feasible joint torque.

First, we consider the results for $M = 3$. The wire arrangement obtained is asymmetric and non-trivial. In Design-1, the feasible joint torque space becomes quite small at certain joint angles, while this is improved in Design-2. When N is increased to 3, for example, Design-1' consists of two wires that simply fold back from Design-1, while the third wire has start and end positions that differ somewhat. Design-2' is mostly a design where the wires from Design-2 are simply folded back. Fundamentally, increasing N from 2 to 3 should double the tension of each wire by folding it back, and thus, the radius of the inscribed hypersphere should also double. Therefore, based on the definition in Eq. 15, a design solution with E_{torque} increased by 2^4 , or 16 times, is possible. Indeed, comparing Design-2 and Design-2', we see that E_{torque} is approximately 16 times larger, as the design is essentially a folded version of the original. On the other hand, Design-1' exhibits an even greater increase in E_{torque} compared to Design-1, demonstrating the effectiveness of the increased design variation afforded by the foldback.

Next, we consider the results for $M = 4$. Here, with four wires allocated to two joints, there is relatively more

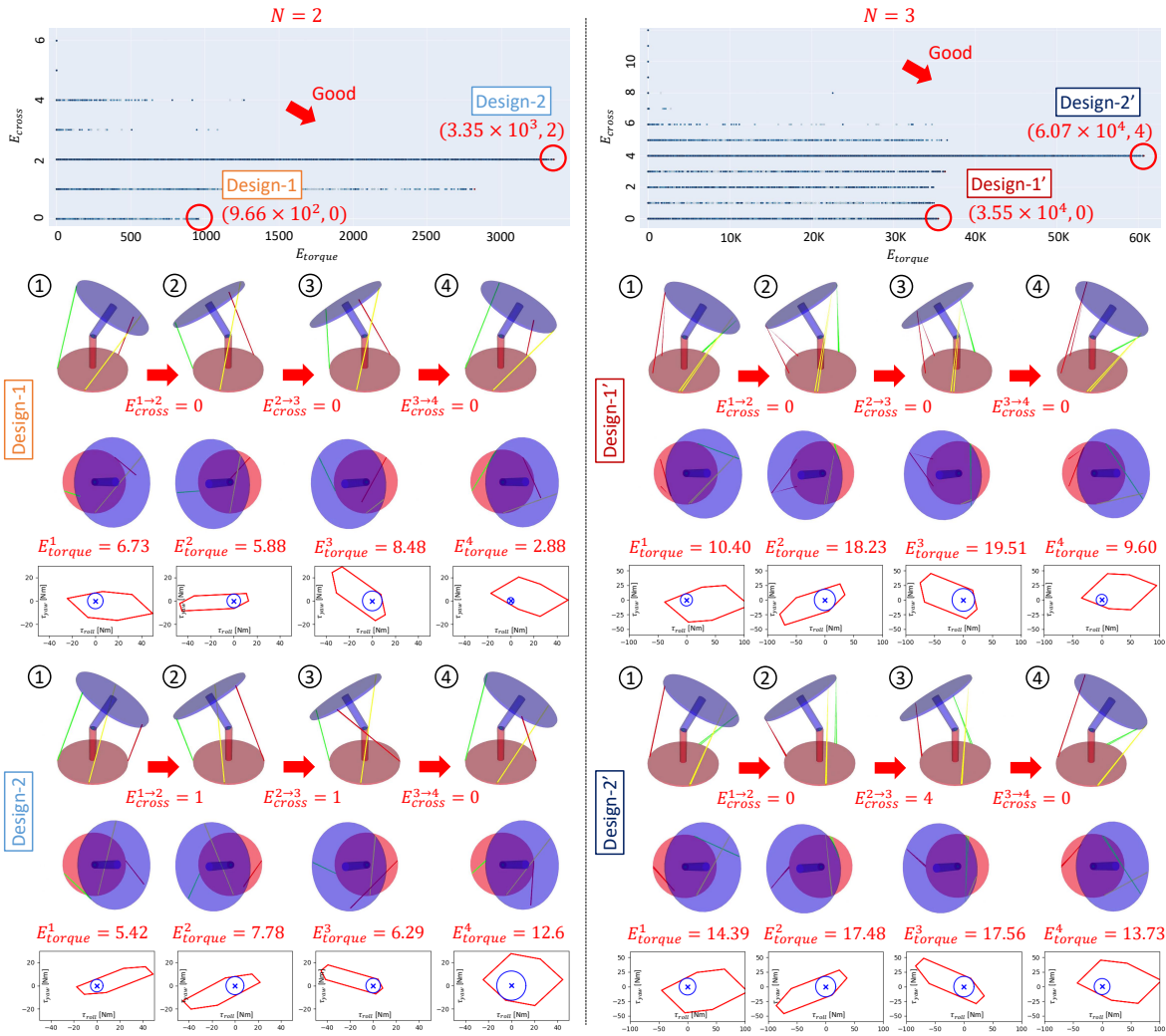


Fig. 5. The sampling results, design solutions, and torque evaluation for simulation experiments on a 2-DOF joint at $N = \{2, 3\}$ and $M = 3$.

flexibility in wire placement, allowing for larger inscribed hypersphere radii at all joint angles. Additionally, the four-wire setup enables symmetrical designs, resulting in all Pareto solutions being symmetric. Because of the symmetric design, there is less interference between wires, and as a result, the E_{torque} values for Design-1 and Design-2 are relatively close. When $N = 3$, the start and end positions of each wire are not significantly different, resulting in a configuration that appears to fold the wires back. Indeed, by increasing N from 2 to 3, we observe that E_{torque} increases by approximately 16 times.

C. 3-DOF Joint Experiments

Fig. 7 shows the results for $N = \{2, 3\}$ and $M = 4$, Fig. 8 shows the results for $N = \{2, 3\}$ and $M = 5$, and Fig. 9 shows the results for $N = \{2, 3\}$ and $M = 6$. For $M = 4$, only the solutions Design-1 and Design-1' are shown, and for $M = \{5, 6\}$, only the Design-1 solutions are shown. From the Pareto solutions, we can see that symmetric designs are observed for $M = 4$ and $M = 6$, whereas no symmetry is observed in the designs for $M = 5$.

For $M = 4$, there is only one Pareto solution for both $N = 2$ and $N = 3$, and we can see that allowing wire crossings

does not lead to further improvement in the solution. When $N = 3$, the start and end points of each wire are so closely aligned that it is difficult to notice any difference in the design solutions. By increasing N from 2 to 3, according to the definition in Eq. 15, it is possible to obtain a design solution with E_{torque} that is 2^8 , or 256 times larger. In fact, Design-1' has an E_{torque} approximately 256 times larger than Design-1, indicating that the effect of allowing wire foldback yields minimal benefit.

For $M = \{5, 6\}$, we obtain highly complex design solutions that are beyond what a human could easily conceive. By increasing N from 2 to 3, E_{torque} increases by approximately 256 times, resulting in a design where the wires are mostly folded back without significant changes to their original configuration.

IV. DISCUSSION

Throughout the study, we found that by varying the number of wires and the degrees of freedom of the joints, it is possible to obtain complex and diverse three-dimensional wire arrangements. Notably, when the number of wires is odd, we obtain unique design solutions lacking symmetry, which are difficult for humans to conceive. In contrast,

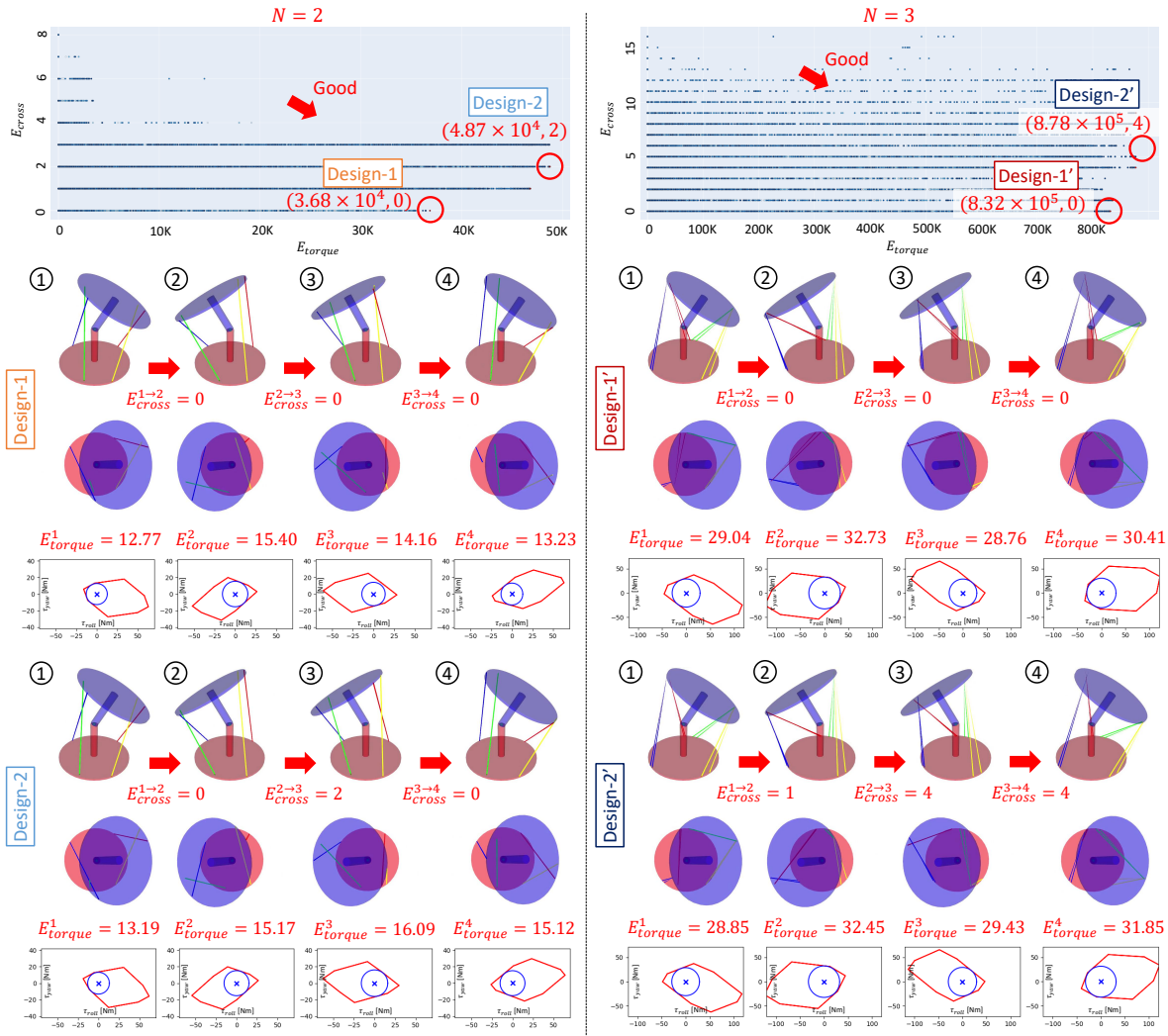


Fig. 6. The sampling results, design solutions, and torque evaluation for simulation experiments on a 2-DOF joint at $N = \{2, 3\}$ and $M = 4$.

when the number of wires is even, the solutions tend to be symmetrical and aesthetically pleasing. By preventing wire crossings, we can obtain design solutions that are feasible for actual hardware implementation. On the other hand, solutions that allow wire crossings often yield better performance. This outcome, however, depends on the problem setup, as there are cases where the best performance is achieved without wire crossings, or where performance does not significantly change whether wire crossings are allowed or not. Additionally, in the settings of this study, increasing the number of relay points for wires rarely led to performance improvement, and the optimal solutions often involved simply folding the wire back directly. While some performance improvements were observed, their impact was small compared to the increased complexity of the design.

The link structure in this study uses a general shape, without delving into the specifics, because further adjustments are required to link lengths, thicknesses, and even the overall structure itself due to hardware constraints, when designing an actual robot. However, We will describe the behavior trends from preliminary experiments when changing the link structure parameters, particularly R , L , and the joint angle

range. Increasing R makes wire placement easier, but it narrows the feasible joint angle range. Increasing L makes wire placement more difficult and increases the likelihood of wire crossings. Regarding the joint angle range, the experiment was conducted within a narrow range of 20 or 30 degrees. However, expanding the range further often leads to situations where no solution can be found that maintains joint torque throughout the entire trajectory, especially when the number of wires is small. Therefore, in this study, the joint angle range and motion trajectory were chosen to ensure that a reasonable solution can be found.

V. CONCLUSION

We proposed a method for three-dimensional wire arrangement optimization considering wire crossings using black-box multi-objective optimization. Previously, wire arrangement optimization had been applied only to relatively simple systems, such as those in two-dimensional planes or systems with constant moment arms where wire crossings did not need to be considered. However, our study removes these constraints, making it applicable to more complex structures. We represented the wire arrangement by defining

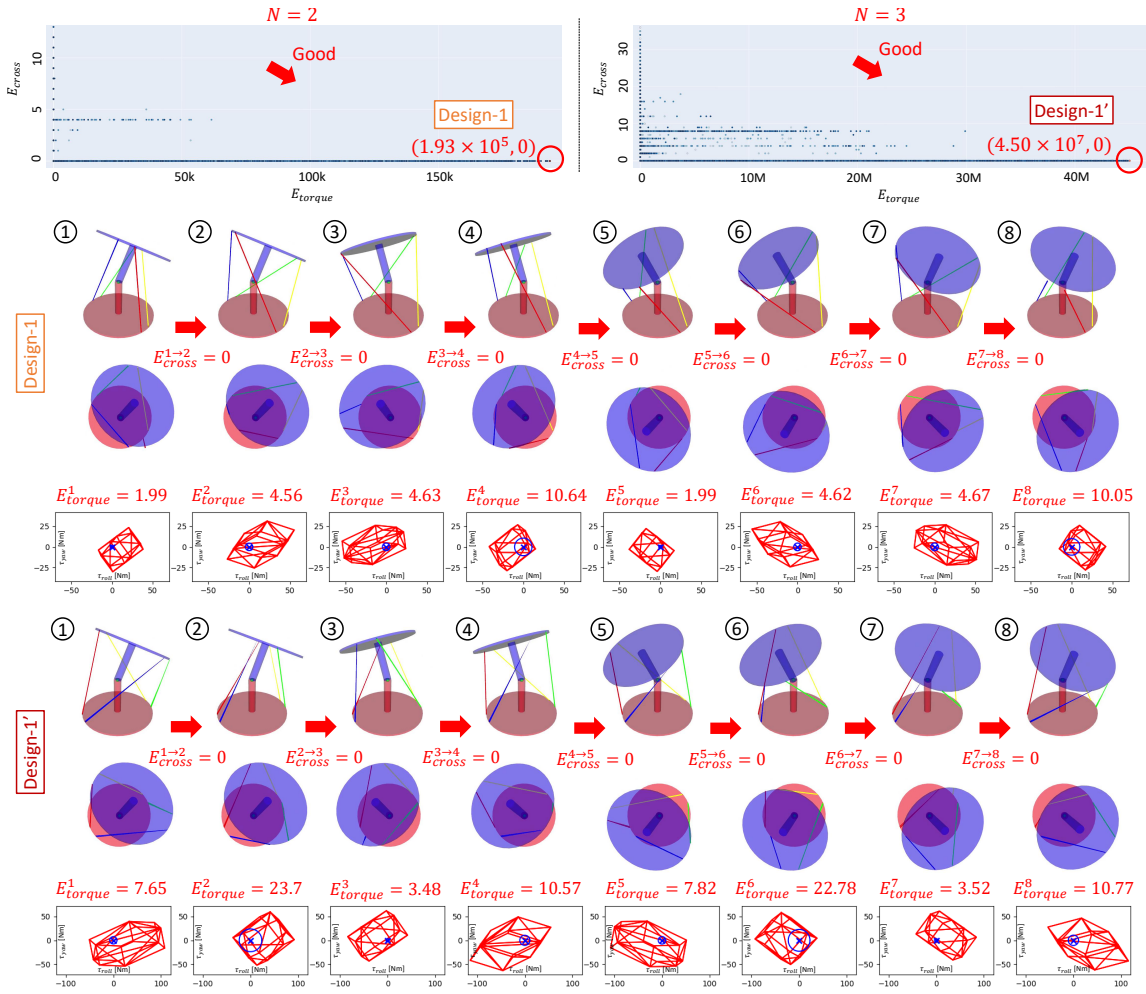


Fig. 7. The sampling results, design solutions, and torque evaluation for simulation experiments on a 3-DOF joint at $N = \{2, 3\}$ and $M = 4$.

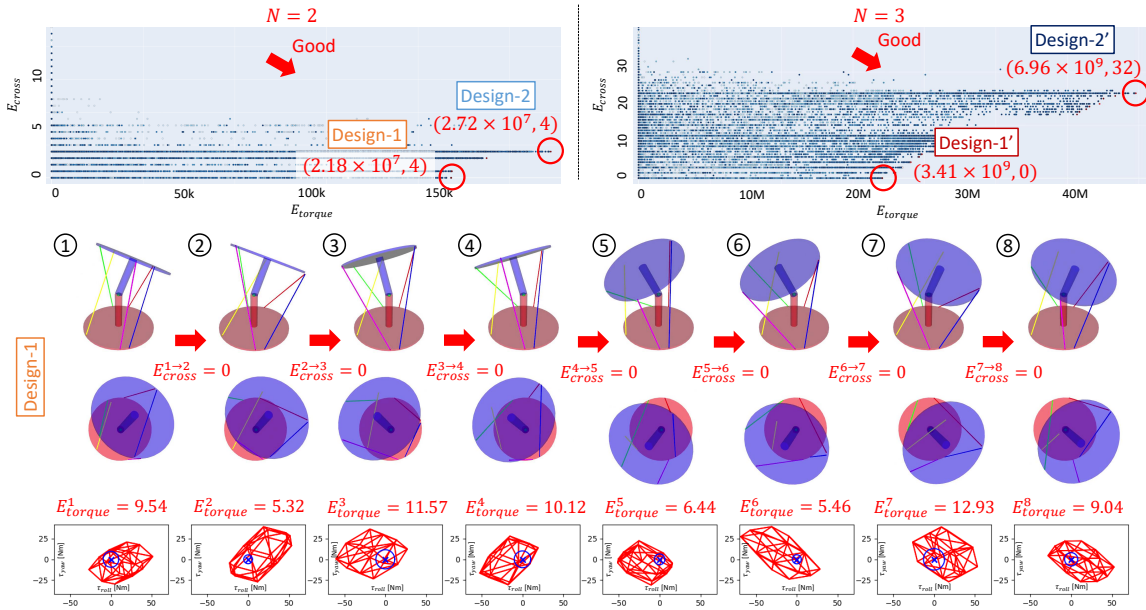


Fig. 8. The sampling results, design solutions, and torque evaluation for simulation experiments on a 3-DOF joint at $N = \{2, 3\}$ and $M = 5$.

the start, relay, and end points of the wires, and geometrically detected wire crossings along the target trajectory, using their count as an evaluation function in the multi-objective

optimization. Additionally, we maximized the product of the radii of hyper-spheres inscribed within the joint torque space for each posture, thereby achieving stable movement along

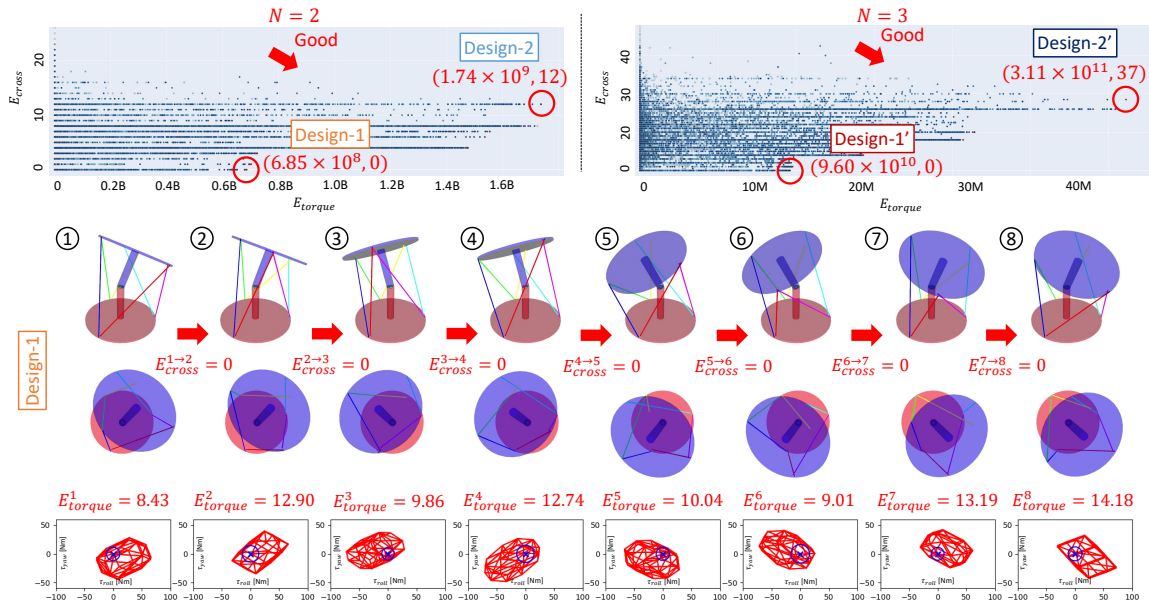


Fig. 9. The sampling results, design solutions, and torque evaluation for simulation experiments on a 3-DOF joint at $N = \{2, 3\}$ and $M = 6$.

the desired trajectory. We successfully optimized the wire arrangement under various conditions for a three-dimensional link structure, which directly extends the planar wire arrangement optimization into three dimensions, obtaining a body design capable of achieving the target trajectory stably while preventing wire crossings.

REFERENCES

- [1] M. Jäntsch, S. Wittmeier, K. Dalamagkidis, A. Panos, F. Volkart, and A. Knoll, "Anthrob - A Printed Anthropomorphic Robot," in *2013 IEEE-RAS International Conference on Humanoid Robots*, 2013, pp. 342–347.
- [2] Y. Asano, T. Kozuki, S. Ookubo, M. Kawamura, S. Nakashima, T. Katayama, Y. Iori, H. Toshinori, K. Kawaharazuka, S. Makino, Y. Kakiuchi, K. Okada, and M. Inaba, "Human Mimetic Musculoskeletal Humanoid Kengoro toward Real World Physically Interactive Actions," in *2016 IEEE-RAS International Conference on Humanoid Robots*, 2016, pp. 876–883.
- [3] K. Kawaharazuka, S. Makino, K. Tsuzuki, M. Onitsuka, Y. Nagamatsu, K. Shinjo, T. Makabe, Y. Asano, K. Okada, K. Kawasaki, and M. Inaba, "Component Modularized Design of Musculoskeletal Humanoid Platform Musashi to Investigate Learning Control Systems," in *2019 IEEE/RSJ International Conference on Intelligent Robots and Systems*, 2019, pp. 7294–7301.
- [4] G. Endo, A. Horigome, and A. Takata, "Super Dragon: A 10-m-Long-Coupled Tendon-Driven Articulated Manipulator," *IEEE Robotics and Automation Letters*, vol. 4, no. 2, pp. 934–941, 2019.
- [5] Y. Kim, "Design of low inertia manipulator with high stiffness and strength using tension amplifying mechanisms," in *2015 IEEE/RSJ International Conference on Intelligent Robots and Systems*, 2015, pp. 5850–5856.
- [6] T. Suzuki, M. Bando, K. Kawaharazuka, K. Okada, and M. Inaba, "SAQIEL: Ultra-Light and Safe Manipulator with Passive 3D Wire Alignment Mechanism," *IEEE Robotics and Automation Letters*, vol. 9, no. 4, pp. 3720–3727, 2024.
- [7] S. Inoue, K. Kawaharazuka, T. Suzuki, S. Yuzaki, K. Okada, and M. Inaba, "CubiX: Portable Wire-Driven Parallel Robot Connecting to and Utilizing the Environment," in *2024 IEEE/RSJ International Conference on Intelligent Robots and Systems*, 2024, pp. 1296–1301.
- [8] N. S. Pollard and R. C. Gilbert, "Tendon arrangement and muscle force requirements for human-like force capabilities in a robotic finger," in *2002 IEEE International Conference on Robotics and Automation*, 2002, pp. 3755–3762.
- [9] T. Asaoka, M. Kawamura, S. Kumakura, and I. Mizuuchi, "Determining the optimal multiarticular muscle arrangement of a musculoskeletal robot for a specific motion using dynamics simulation," in *2012 IEEE-RAS International Conference on Humanoid Robots*, 2012, pp. 216–221.
- [10] W. Roozing, Z. Li, D. G. Caldwell, and N. G. Tsagarakis, "Design Optimisation and Control of Compliant Actuation Arrangements in Articulated Robots for Improved Energy Efficiency," *IEEE Robotics and Automation Letters*, vol. 1, no. 2, pp. 1110–1117, 2016.
- [11] H. Dong, E. Asadi, C. Qiu, J. Dai, and I. Chen, "Geometric design optimization of an under-actuated tendon-driven robotic gripper," *Robotics and Computer-Integrated Manufacturing*, vol. 50, pp. 80–89, 2018.
- [12] K. Kawaharazuka, Y. Toshimitsu, M. Nishiura, Y. Koga, Y. Omura, Y. Asano, K. Okada, K. Kawasaki, and M. Inaba, "Design Optimization of Musculoskeletal Humanoids with Maximization of Redundancy to Compensate for Muscle Rupture," in *2021 IEEE/RSJ International Conference on Intelligent Robots and Systems*, 2021, pp. 3204–3210.
- [13] S. Islam, Z. He, and M. Ciocarlie, "Task-Based Design and Policy Co-Optimization for Tendon-driven Underactuated Kinematic Chains," in *2024 IEEE/RSJ International Conference on Intelligent Robots and Systems*, 2024.
- [14] P. Berthet-Rayne and K. Leibrandt and K. Kim and C. A. Seneci and J. Shang and G. Yang, "Rolling-Joint Design Optimization for Tendon Driven Snake-Like Surgical Robots," in *2018 IEEE/RSJ International Conference on Intelligent Robots and Systems*, 2018, pp. 4964–4971.
- [15] I. B. Hamida, M. A. Laribi, A. Mlika, L. Romdhane, S. Zeghloul, and G. Carbone, "Multi-Objective optimal design of a cable driven parallel robot for rehabilitation tasks," *Mechanism and Machine Theory*, vol. 156, pp. 1–24, 2021.
- [16] H. Jamshidifar, A. Khajepour, B. Fidan, and M. Rushton, "Kinematically-Constrained Redundant Cable-Driven Parallel Robots: Modeling, Redundancy Analysis, and Stiffness Optimization," *IEEE/ASME Transactions on Mechatronics*, vol. 22, no. 2, pp. 921–930, 2017.
- [17] S. Zhong, J. Zhou, and W. Wu, "Constructing Constraint Force Field in Musculoskeletal Robot by Co-optimizing Muscle Arrangements and Constant Activations," in *2022 International Joint Conference on Neural Networks*, 2022, pp. 1–7.
- [18] K. Kawaharazuka, S. Yoshimura, T. Suzuki, K. Okada, and M. Inaba, "Design Optimization of Wire Arrangement with Variable Relay Points in Numerical Simulation for Tendon-Driven Robots," *IEEE Robotics and Automation Letters*, vol. 9, no. 2, pp. 1388–1395, 2024.
- [19] R. P. Brent, *Algorithms for minimization without derivatives*. Courier Corporation, 2013.
- [20] T. Akiba, S. Sano, T. Yanase, T. Ohta, and M. Koyama, "Optuna: A Next-generation Hyperparameter Optimization Framework," in *25th ACM SIGKDD International Conference on Knowledge Discovery and Data Mining*, 2019.